JOURNAL OF CATALYSIS 116, 568–585 (1989)

Morphology of Graphite-Supported Iron–Manganese Catalyst Particles: Formation of Hollow Spheres during Oxidation

A. A. CHEN, M. A. VANNICE, AND J. PHILLIPS[1]

Department of Chemical Engineering, The Pennsylvania State University, 133 Fenske Laboratory, University Park, Pennsylvania 16802

Received August 23, 1988; revised November 15, 1988

Transmission electron microscopy (TEM) and Mössbauer spectroscopy (MES) were used to study the morphology of graphite-supported iron–manganese particles. Following oxidation at 500 K MES showed the iron in the particles to be fully oxidized. TEM showed all the particles to be torroidal in appearance. However, tilting resulted in no change in the apparent dimensions of the particles, yet the apparent distances between particles were sharply reduced. These results suggest the particles are actually spherical. On the basis of these experiments, and similar experiments with reduced particles, a model was developed: Following reduction the particles are spherical and consist of a metallic iron core surrounded by a shell of manganese oxide. During oxidation, iron ions diffuse through the manganese oxide shell to the particle surface. Eventually, this results in the formation of nearly spherical particles with hollow centers, inner shells of iron–manganese spinel, and outer shells of iron oxide. Upon an additional reduction the hollow center remains, but the shells phase segregate into regions of iron metal and manganese oxide.

INTRODUCTION

Manganese-promoted iron catalysts are known to be excellent Fischer–Tropsch catalysts, since they are more selective for olefins than unpromoted iron (*1–3*). Catalysts derived from Fe–Mn carbonyl clusters dispersed on carbon are of particular interest because of their high selectivity to low-molecular-weight olefins (*4*).

In order to understand the special chemistry of these catalysts, a number of studies of structure have been undertaken (*3–14*). It has been found that the particles exhibit complex structural behavior which is a function of temperature and gas composition. After initial calcination in air or following any high-temperature oxidation treatment, it is generally agreed that most of the metal is present as one or more forms of Fe/Mn oxide, the precise composition depending on the starting Fe/Mn ratio (*3, 7*). Following high-temperature reduction in hydrogen, an iron-rich and a manganese-rich phase form, and again the compositions are a function of the starting Fe/Mn ratio (*7, 12*). In iron-rich catalysts, for example, the two phases are generally understood to be α-Fe and a MnO phase which contains some FeO impurity (*14*). Moreover, the MnO phase is thought to cover the α-Fe phase (*3, 10, 11, 14*).

Under Fischer–Tropsch reaction conditions there are conflicting reports regarding the phases present and the identity of the active phase. Jensen and Massoth (*14*) reported that α-Fe and MnO were the principal active phases, which were the same phases they found under reduction conditions. They reported that only a small amount of iron carbide formed, and they suggested that the manganese in the particles act only as a catalytic "promoter," decreasing the specific Fischer–Tropsch activity and changing the selectivity of the Fe phase. In contrast, Van Dijk *et al.* (*15*) reported that virtually all the Fe was converted to carbide under reaction conditions, and the Mn remained in the form of MnO. Yet another group (*6, 7*) suggested

[1] To whom correspondence should be addressed.

0021-9517/89 $3.00

that the exact phases present under reaction conditions are a function of a number of parameters including pretreatment conditions, gas phase composition, and temperature. In all cases they found at least some nonstoichiometric $Fe_{3-x}Mn_xO_4$ mixed spinel to be present, and they contend that the Mn oxide phase reduces the rate of Fe carburization and thus enhances catalyst lifetime.

Although progress has been made in understanding the complexities of the Fe–Mn system, many questions remain unanswered. For example, the structural arrangement of the various phases present in the particles remains unknown. Furthermore, the influence of treatment on the structure remains unclear. In the present study, an effort was made to understand the structural changes which take place in Fe–Mn particles as a result of reduction and oxidation treatments. Specifically, the structure of Fe–Mn particles formed on a graphitic support via the thermal decomposition of a mixed-metal carbonyl cluster precursor was studied using Mössbauer spectroscopy (MES), X-ray diffraction (XRD), and transmission electron microscopy (TEM).

Recent work on the structure of Fe–Rh catalyst particles demonstrated the advantages of using noninteractive supports for the study of bimetallic catalyst particles (*16*). The minimal interaction between the graphite support and the metals means that particle–support interactions will not strongly influence morphology, thus removing a source of ambiguity in the data analysis. The minimal interaction also results in the formation of larger particles which give less "relaxed" Mössbauer spectra (*17*) and narrower lines in the XRD measurements.

On the basis of the results obtained in the present study, a model of Fe–Mn particle structure following reduction and oxidation treatments was developed. It is suggested that hydrogen reduction at 673 K results in the formation of spherical particles with a metallic Fe core and a surrounding shell which is predominantly MnO. During high-temperature oxidation, it is proposed that diffusion of Fe ions through the MnO layer leads to the formation of an inner shell of Fe_2MnO_4 and an outer shell of γ-Fe_2O_3. This diffusional process leaves a spherical void space at the center of approximately spherical particles. The structures cannot be "cycled"; that is, following the oxidation step, a subsequent reduction leads to a breakdown of the outer shells into small particles of metallic Fe and MnO, but the center void space remains.

EXPERIMENTAL PROCEDURE

Catalyst Preparation

Grafoil (Union Carbide), the catalyst support used in the present study, is a highly graphitic, very pure carbon with a relatively low average surface area of 22 m^2/g, nearly all of which exists as highly uniform basal plane surface (*18–21*). Prior to metal impregnation, the Grafoil was ground and then pretreated in flowing H_2 for 12 h at 1223 K. After being cooled in the H_2 flow to room temperature, it was transferred without exposure to air to a nitrogen-purged glovebox. $N[(C_2H_5)_4]Fe_2Mn(CO)_{12}$ was prepared in accordance with a previously published procedure (*22*) and then dissolved in dried, degassed THF. This solution was added dropwise to the continuously stirred Grafoil under a nitrogen atmosphere using standard Schlenk techniques (*23*). Following impregnation the THF was removed from the catalyst by evacuation at 0.13 Pa and 298 K for 8 h. It is important to note that at no point in this procedure was the catalyst exposed to oxygen. The final weight loading of the catalyst was found to be 6.4 wt% total metal and 4.4 wt% Fe. For control purposes, Fe-only and Mn-only catalysts were prepared in an identical fashion using $Fe_3(CO)_{12}$ (Pressure Chemical Co.) and $Mn_2(CO)_{10}$ (Pressure Chemical Co.), respectively, as the catalyst precursors.

Mössbauer Spectroscopy

The MES system has been described in detail elsewhere (*24*). It consists of electronics and data handling system from Austin Science Associates Inc. and a stainless-steel cell with Kapton windows capable of being operated at temperatures ranging from 77 to 700 K and pressures ranging from 0.1 MPa to 1.3×10^{-3} Pa. The cell is attached to a standard glass high-vacuum/gas handling system. Following drying the samples were placed without air exposure in the Mössbauer cell and all further treatments were conducted *in situ* either under vacuum or in flowing gases at 0.1 MPa. For the 10 K spectra, air-exposed samples were placed in an Air Products Helitran liquid He-cooled Mössbauer cell which was evacuated during data collection.

The spectra were analyzed with the program MFIT (*25*) which fits the data to an assigned number of Lorentzian lines superimposed on a flat baseline. The fitting is "least squares" and employs a random stepping of free parameters. All sextuplets were constrained such that (i) the separations between lines were consistent with the known nuclear magnetic moment of Fe and (ii) the dips and widths of peaks at negative velocity were equal to those of corresponding peaks at positive velocity. In sum, the free parameters are the quadrupole splittings, hyperfine fields, and isomer shifts. All of the spectra were collected in the constant acceleration mode and all isomer shifts are reported with respect to α-Fe.

X-Ray Diffraction

X-ray diffraction measurements were performed on air-exposed samples using a Rigaku Model 4011B3 diffractometer. Prior to mounting into the diffractometer the samples were pressed into pellets at approximately 10,000 psi (69 MPa). As shown in an earlier study (*26*), this has the effect of aligning the basal planes of the Grafoil, thus greatly simplifying the diffraction pattern.

Transmission Electron Microscopy

TEM studies of air-exposed samples were conducted at 120 kV with a Philips 420 STEM microscope equipped with a Link Systems energy-dispersive X-ray analyzer (EDS). Particularly crucial to the experiments described later was the fact that the specimen stage could be tilted between the angles of $-35°$ and $+35°$ relative to horizontal. For EDS analyses, the stage was tilted at $-30°$ and the electron beam was focused to a 70-nm spot which was placed on the area to be analyzed.

So that particular particles could be studied sequentially in the electron microscope as a function of pretreatment, six specimens were prepared on heat-resistant Mo grids as follows. After the first reduction treatment at 673 K (see below), some of the catalyst was attached to replica tape and then thinned by repeated removing of layers of Grafoil with adhesive tape, using a method similar to that described elsewhere (*27*). The replica tape with the thinned Grafoil flakes was cut into 2 × 2-mm squares, and each square placed on a 200-mesh Mo grid. The replica tape was then dissolved using acetone vapor.

Some of the particles on each of the "gridded" samples were selected for study as a function of pretreatment Specifically, after the first reduction (and ambient atmosphere exposure) certain particles, chosen because they represented a particular class (i.e., large or small, isolated or "clumped") of particles, were examined as a function of tilt angle. The gridded samples were then placed in a simple glass flow reactor, oxidized, and then returned (following ambient atmosphere exposure) to the microscope, where the previously studied individual particles were relocated and reexamined as a function of stage tilt angle. This process was repeated for a final time after the samples had undergone a second reduction treatment. Details of the treatment times and temperatures are given in Table 1. The MES sample and the gridded samples were

TABLE I

Reduction and Oxidation Pretreatments

1. Initial Reduction: Flow H_2 over catalyst, raise temperature to 673 K, reduce at 673 K for 16 h, cool to 298 K in H_2 flow.
2. High-temperature Oxidation: Flow O_2 over catalyst, raise temperature to 523 K, oxidize for 14 h at 523 K, cool to 298 K in O_2 flow.
3. Re-reduction: Flow H_2 over catalyst, raise temperature to 673 K, reduce at 673 K for 16 h, cool to 298 K in H_2 flow.

given identical treatments and, after the oxidation step, part of the MES sample was examined in the TEM. This examination indicated that the particles in the MES sample were similar to those observed for the gridded samples.

The purpose of the tilting studies of the gridded samples was to determine particle shape, specifically to determine if they were nearly spherical or closer to being flat in shape. The appearance of spherical particles will not change significantly upon tilting. In contrast, truly flat particles will appear shorter in the direction perpendicular to the axis of tilt, in proportion to the cosine of the tilt angle. There are two determinations—true horizontal orientation and axis of tilt—which must be made for this technique to give quantitative results, but neither is difficult to determine in practice. The axis of tilt can be found by measuring distances between objects along a number of different lines as a function of specimen stage tilt and by determining the particular direction along which the line distances shorten in proportion to the cosine of the tilt angle. The tilt axis will be perpendicular to that direction. The true horizontal orientation can be found by noting the tilt angle at which apparent distances between objects start to increase instead of decrease. It is important to note that the zero tilt angle of the specimen stage and the horizontal orientation of Grafoil flakes do not correspond in general; in fact, the true horizontal orientation is sometimes completely outside the 70° tilting range of the specimen stage. In this case the cosine rule predicts that the maximum foreshortening of distances perpendicular to the tilt axis will be achieved when tilting is done through the full allowed range of 70°, and apparent distances between objects will continuously increase/decrease between the tilt limits of the stage. Apparent distances along the perpendicular to the tilt axis at one end of the range will be 34% (cos 70°) of those at the other end. In the case where the stage horizontal and the sample horizontal exactly correspond, the apparent maximum foreshortening will be the smallest. That is, at either end of stage travel (±35°), distances between objects will be 82% of those at zero tilt.

RESULTS

The samples were subjected to a simple series of reduction and oxidation treatments (see Table 1). After each treatment the morphology of selected particles on the gridded samples was studied by TEM, while the Fe phases in the Fe–Mn sample were studied using MES. The results of characterization following each treatment are presented below.

Reduction at 673 K

A Mössbauer spectrum of the Fe–Mn sample following reduction in flowing H_2 at 673 K for 16 h is shown in Fig. 1a. The spectrum is unrelaxed and has parameters characteristic of α-Fe (Table 2). This suggests that most of the Fe in the samples was present as large α-Fe particles in which no Mn was incorporated.

TEM studies of the gridded samples following reduction and air exposure revealed that there were two types of particle morphologies. Particles smaller than about 10 nm in diameter appeared to have a "ring" structure (region 1, Fig. 2); that is, they were roughly circular in shape with a light center and a dark outer ring. Larger particles (Fig. 3 and Fig. 2, region 2) appeared

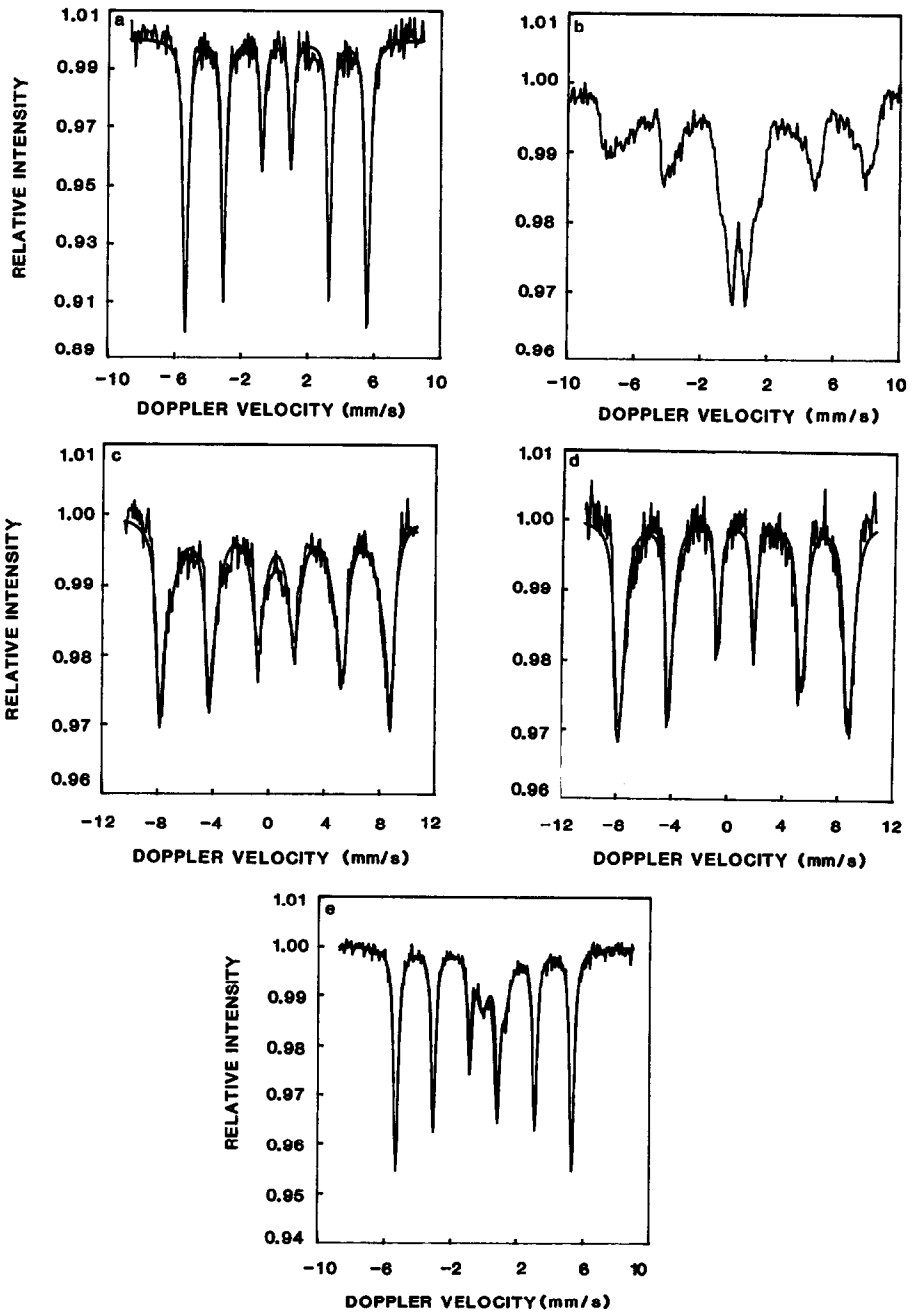

FIG. 1. (a) Mössbauer spectrum (77 K) of Fe–Mn catalyst after reduction in H_2 at 673 K for 16 h. (b) Mössbauer spectrum (298 K) of sample in (a) after oxidation in pure O_2 at 523 K for 14 h. (c) Same sample as (b), collected at 77 K. (d) Same sample as (b), collected at 10 K. (e) Mössbauer spectrum (298 K) of sample in (b) after re-reduction in H_2 at 673 K for 16 h. Mössbauer parameters are shown in Table 2.

TABLE 2

Mössbauer Parameters for Fe–Mn/Graphite Catalyst

Pretreatment	Figure	Temp.	Assignment	I.S. (mm/s)	Q.S. (mm/s)	H (kOe)	% Area
673 K/16 h in H_2	1a	77	α-Fe	0.1	0.0	340.0	100.0
523 K/14 h in O_2	1c	77	Oxide (I)	0.5	0.0	516.0	57.4
			Oxide (II)	0.4	0.0	478.0	42.6
523 K/14 h in O_2	1d	10	Oxide (I)	0.5	−0.1	520.7	37.8
			Oxide (II)	0.5	0.0	500.5	77.8
673 K/16 h in H_2	1e	298	α-Fe	0.0	0.0	330.5	77.8
			Oxide	0.6	1.3		22.2

roughly circular and had a dark center or were uniformly dark.

For the Fe–Mn sample, EDS studies were performed on 10 isolated particles in an effort to obtain approximate compositions. It was found in all cases that both Fe and Mn were present within the individual particles. On the basis of a large number of tilting experiments it was found that all the particles, both large and small, were roughly spherical. That is, distances between objects varied according to the cosine relation, but the particles themselves did not appear to foreshorten at all and remained approximately circular at all tilt angles. An example of one tilting study is shown in Fig. 3. The finding that the particles were roughly spherical is consistent with a "side view" of the particles as shown in Fig. 3c. For the Fe-only and Mn-only samples, the particles also appeared solid at this stage. An example of the reduced Fe-only particles is shown in Fig. 4.

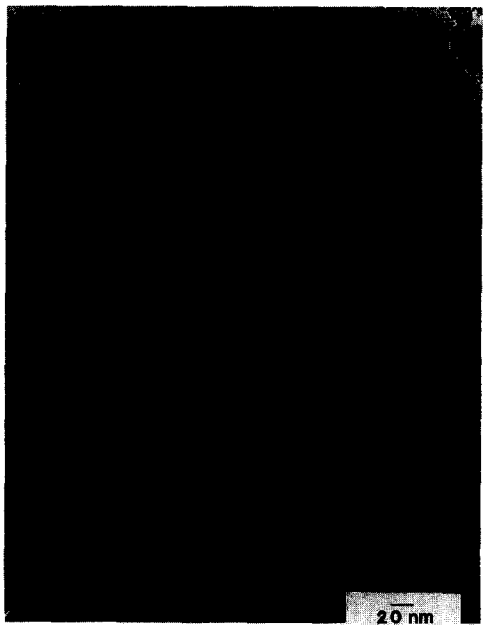

FIG. 2. Transmission electron micrograph of Fe–Mn catalyst after initial reduction and air exposure at room temperature. The particles in region 1 are predominantly below 10 nm in diameter and show a "ring-like" structure. The particles in region 2 are larger and appear solid. The particles in this figure were all determined to be roughly spherical, on the basis of tilting experiments between the stage tilt angles of −35° and +35°.

Oxidation at 523 K

Following oxygen treatment for 14 h at 523 K, the MES results on the Fe–Mn sample showed that all of the Fe was oxidized (Figs. 1b, 1c, 1d). At room temperature, the spectrum was partially relaxed, and there was a doublet in the spectrum, indicating that at least some of the particles were small (*17, 18*). No fitting of the relaxed spectrum was attempted, since the unreliability of such results is well known (*28*). At low temperatures (Figs. 1c and 1d), the lines were far less "relaxed," but still broadened and somewhat asymmetric, suggesting the presence of at least two sextuplets. A comparison of the parameters

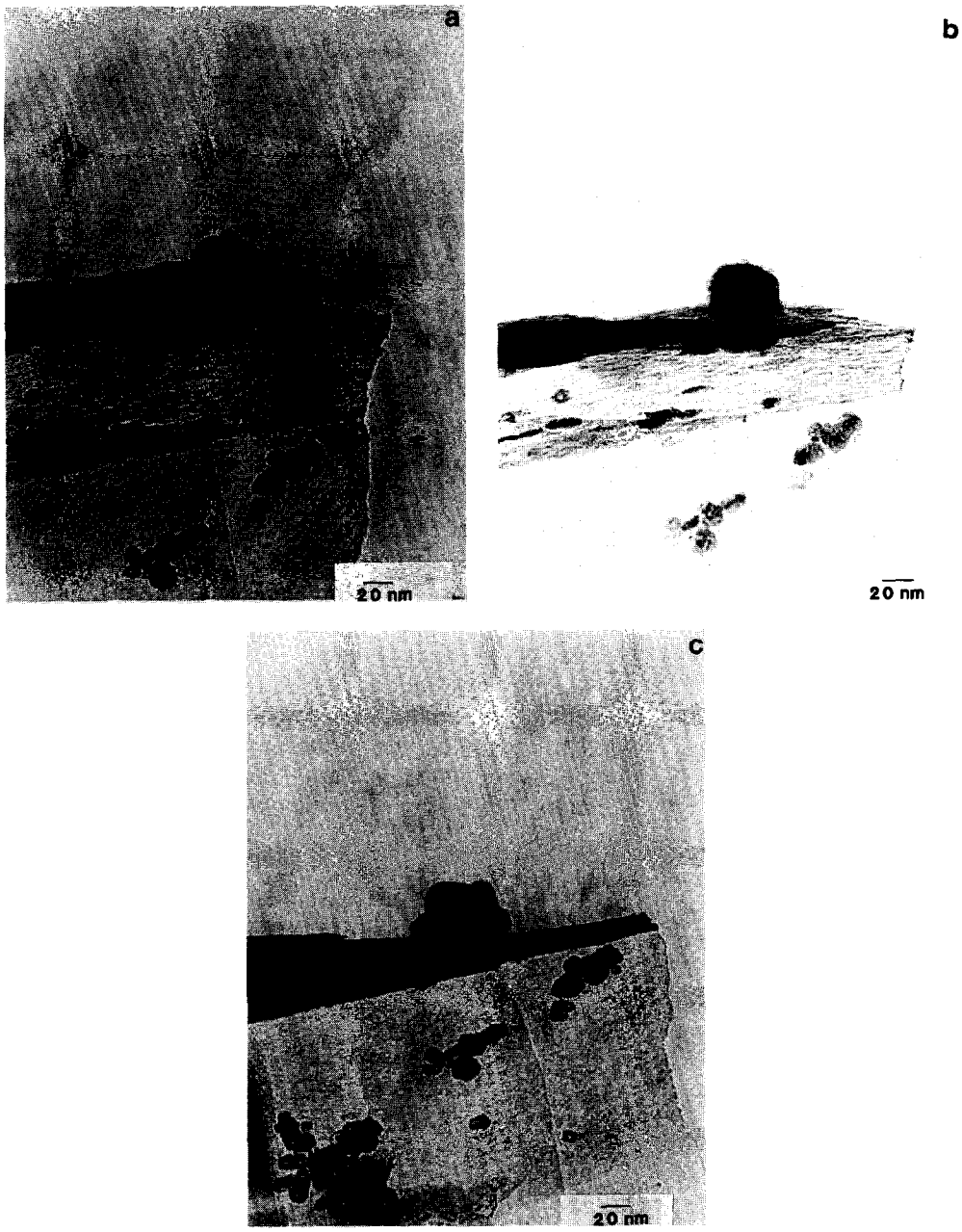

FIG. 3. Representative tilt micrographs on a region of the Fe–Mn catalyst after initial reduction. All tilt angles refer to the microscope stage tilt angle relative to the stage horizontal at 0°; tilt axis is marked TA. (a) +30°; (b) +25°; (c) +18°. Micrograph (c) shows the particles "edge on."

obtained in this work (Table 2) with parameters previously obtained on various oxides (Table 3) indicates that α-Fe_2O_3 and/or a mixed oxide species, either Fe_2MnO_4 or $Fe_{2-x}Mn_xO_4$, existed in the oxidized sample. The presence of bulk α-Fe_2O_3 can be ruled out since the hyperfine splitting of that species is 20 kOe greater than the split-

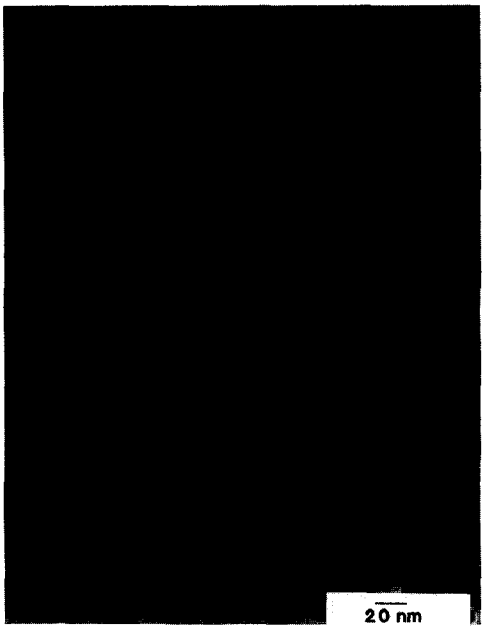

FIG. 4. Micrograph of Fe-only sample after reduction at 673 K and air exposure at 300 K.

tings found here. It is clear that MES alone is not sufficiently sensitive in this case to determine with absolute certainty whether only one or both of these species were present.

In order to obtain further phase information on these samples, they were removed from the MES cell and studied using XRD. It was assumed that air exposure following a high-temperature oxidation had no effect on the phases present. A broad peak for Fe_2MnO_4 and two peaks for α-Fe_2O_3 were detected (Fig. 5). Thus, on the basis of both the XRD and the MES results, it was concluded that both Fe–Mn spinel and α-Fe_2O_3 were present after high-temperature oxidation.

TEM studies showed that following the oxidation procedure, virtually all of the particles had a ring-like appearance, as seen in Figs. 6 and 7, and had noticeably expanded. Tilting studies were conducted to determine the shape of the particles. Figure 7 shows a tilt sequence on the same particles as those in Fig. 3, but after oxidation. It was found that to a good approximation, the overall appearance of the particles was independent of the tilt angle. In some cases, the foreshortening of apparent distances between surface features was quite signifi-

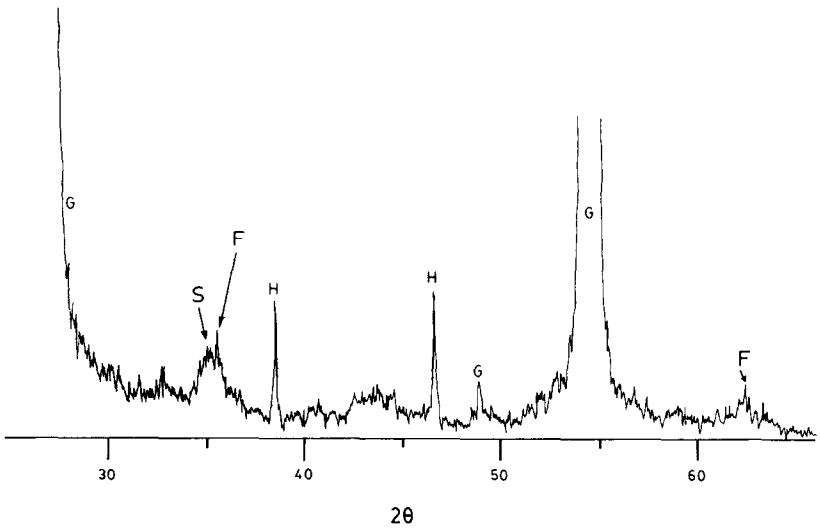

FIG. 5. X-ray diffractogram of the oxidized Fe–Mn catalyst, subsequently air exposed during loading. Peaks resulting from the Grafoil support are marked G. The broad peak at $2\Theta = 35.03°$ (S) corresponds to Fe_2MnO_4, while peaks at $2\Theta = 35.6°$ and $2\Theta = 62.7°$ (F) indicate that some γ-Fe_2O_3 is present. The peaks marked H are from the specimen holder.

TABLE 3

Mössbauer Parameters of Bulk Oxides

Assignment/form	Temp. (K)	I.S. (mm/s)	Q.S. (mm/s)	H (kOe)	Reference
A. Fe_2MnO_4					
Fe_2MnO_4/bulk					
Site (I)	293	0		470 ± 25	(*49*)
Site (II)		0		450 ± 25	
Fe_2MnO_4/bulk	295				(*12*)
Site (I)				493	
Site (II)				443–486	
Fe_2MnO_4/bulk	300	0.5		425	(*50*)
Fe_2MnO_4/bulk					
Site (I)	298			480	(*51*)
Site (II)				456	
Fe_2MnO_4 powder	298				
Site (I)		0.4	−0.1	490.1	This work
Site (II)		0.5	0	438.8	
Fe_2MnO_4/bulk	77	0.1		510 ± 20	(*49*)
B. Fe_2O_3					
γ-Fe_2O_3/bulk					
Site (I)	299			488 ± 5	(*53*)
Site (II)				499 ± 5	
γ-Fe_2O_3/bulk	298	0.3		496 ± 20	(*54*)
α-Fe203/bulk	298			515	(*53*)
α-Fe203/bulk	298			522.2	(*55*)
Fe_2O_3/graphite	298	0.4	−0.1	504.5	This work
γ-Fe203/bulk	85			515 ± 20	(*52*)
α-Fe203/bulk	77			540–544	(*55*)
α-Fe203/bulk	0			544	(*55*)

cant, while the apparent diameter of the particles remained virtually constant, as seen in Fig. 8. The results of the tilt series in Fig. 8 are quantitatively summarized by the plot shown in Fig. 9. As Fig. 9 illustrates, the interparticle distance foreshortens in accordance with the cosine of the relative tilt angle. The diameters of the particles, however, stayed almost constant, consistent with a spherical geometry.

TEM studies of the oxidized Fe-only and Mn-only catalysts showed that the Mn-only particles remained solid (Fig. 10), whereas the Fe-only particles formed voids (Fig. 11). Also, it is important to note that, while the Fe particle diameters expanded by approximately 50% on oxidation, no detectable expansion of the Mn particles occurred. Tilting studies indicated that in both samples the particles were roughly spherical in shape, and the results are summarized in Fig. 12 for the Fe-only sample.

On the basis of all the TEM observations, it is concluded that the particles which appear to have a "ring structure" are, in actuality, nearly spherical in shape. This simple postulate explains the fact that the appearance of the particles is independent of the tilt angle, and the fact that there is no foreshortening of the particles during tilting.

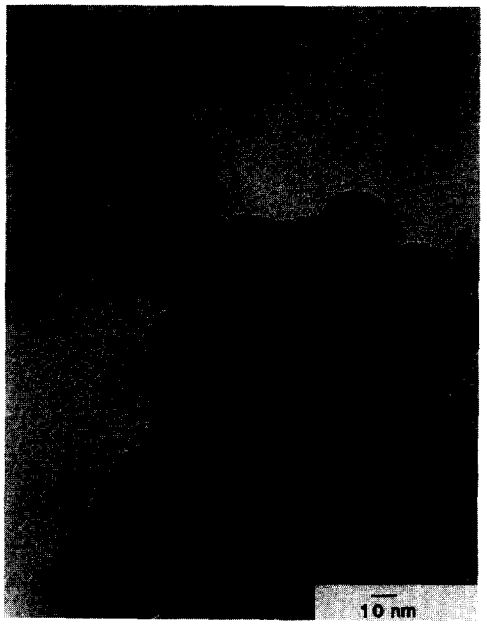

FIG. 6. Micrograph of Fe–Mn sample after oxidation and air exposure at 300 K showing a group of particles. A tilt series on this group of particles showed that the two particles in the upper left were spherical in shape. The overlapping particles all appeared ring-shaped at all tilt angles.

Given that the particles are spherical following both oxidation and reduction, it is reasonable to make a size comparison between particles on the basis of a measurement of diameter. This was done for a number of ring-shaped particles in the Fe–Mn sample, and for the particles that did not appear ring-shaped after the initial reduction, an average diameter enlargement of 39% was observed when compared to the diameter after initial reduction. Particles which were ring-shaped after the initial reduction, for example, those in region 1 of Fig. 2, did not expand after oxidation.

Re-reduction at 673 K

As a final step, the Fe–Mn sample was re-reduced at 673 K for 15 h in flowing H_2. After this treatment the MES results show that α-Fe is the dominant species, although about 20% of the spectral area is in the form of a doublet, typical of a superparamagnetic oxide. The parameters of the α-Fe phase are precisely those of large unrelaxed crystals, indicating that it is unlikely that there

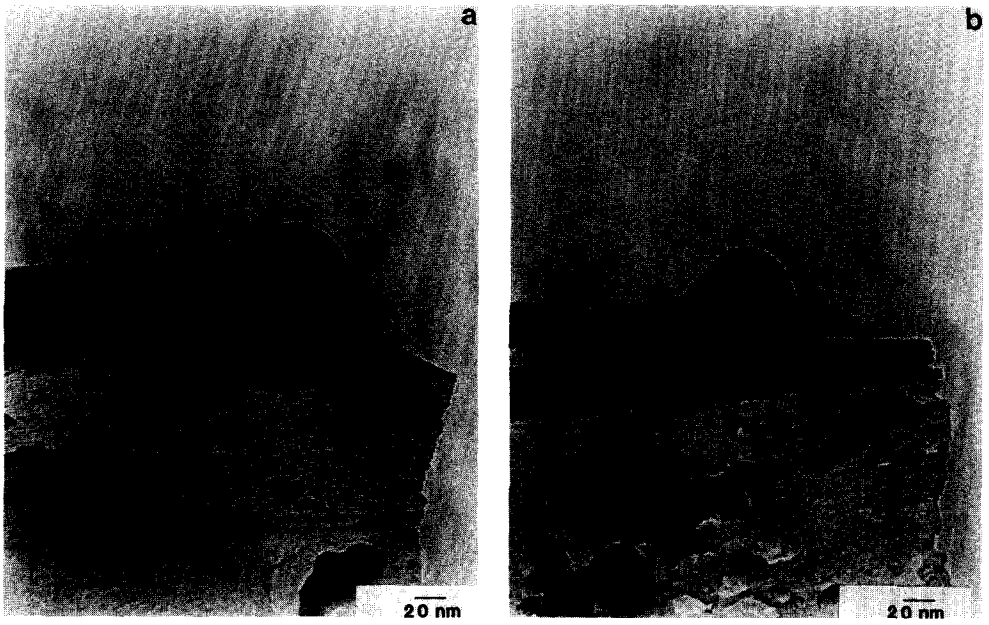

FIG. 7. Representative tilt micrographs of the same region as in Fig. 3, after oxidation at 523 K and exposure to air at 300 K. These pictures were taken at the same magnification as that in Fig. 3 so that the particle expansion could be measured. Tilt angles refer to the microscope stage tilt angle relative to the stage horizontal at 0°. (a) +35°; (b) +15°.

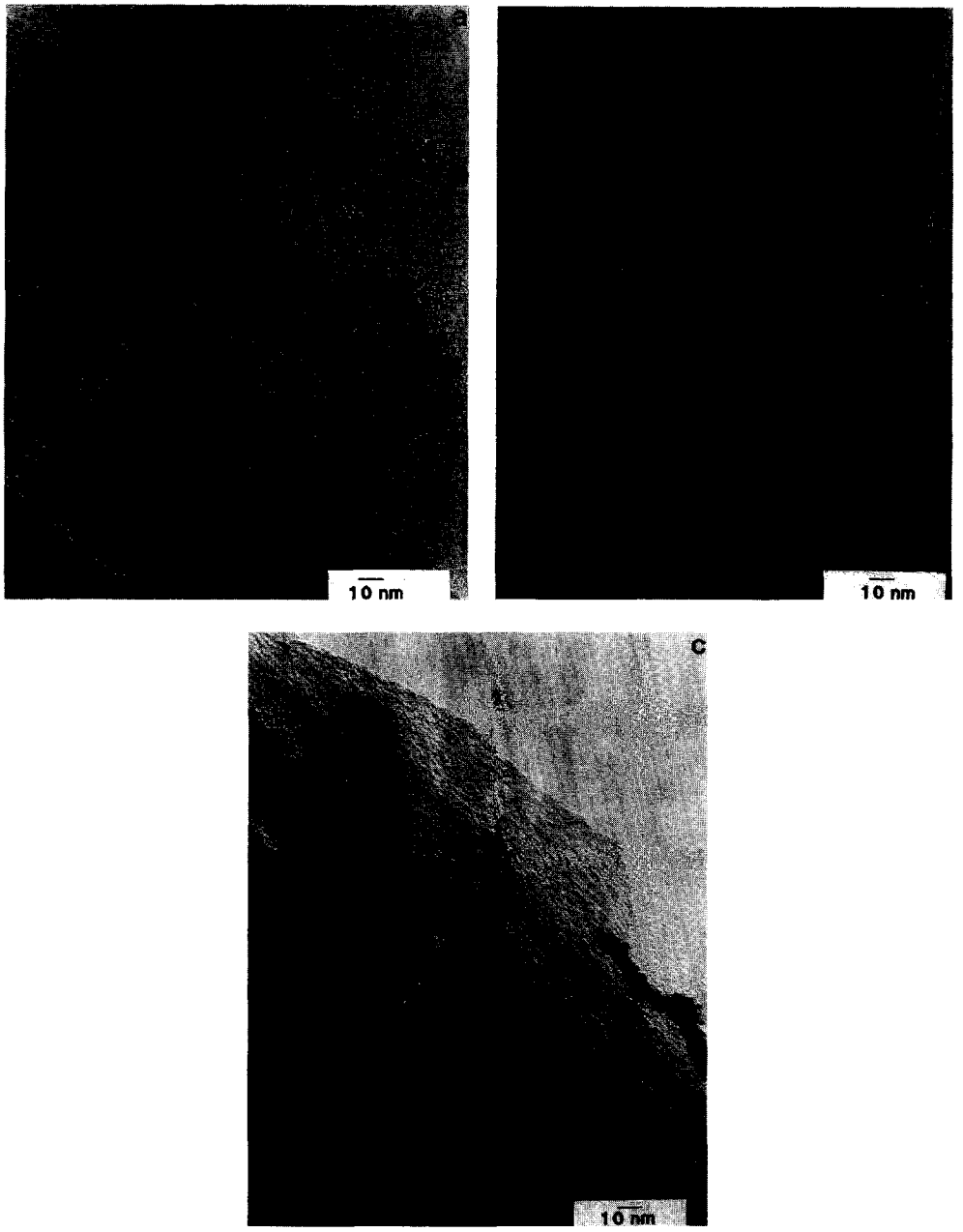

FIG. 8. Representative tilt micrographs on an isolated set of particles after oxidation at 523 K and exposure to air at 300 K. All tilt angles refer to the microscope stage tilt angle relative to the stage horizontal at 0°. The tilt axis is marked TA. (a) +35°; (b) −6°; (c) −35°. In this case the true horizontal of the Grafoil lies outside the tilt limits of the stage. The relative distance between particles A and C shortens in accordance with the cosine of the relative tilt angle, as shown in Fig. 9.

was significant incorporation of Mn into this phase (Table 2). The presence of the doublet is attributed to a small amount of oxidized Fe due to incomplete reduction.

The TEM results show that virtually all the particles remain ring-like in appearance. However, the appearance of the outer part of the ring had changed, appear-

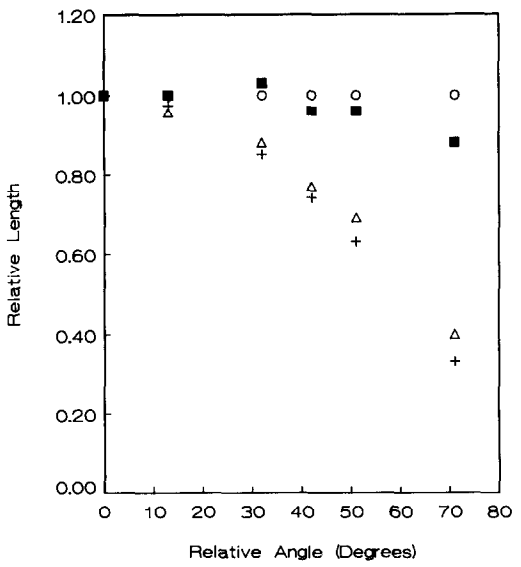

FIG. 9. Plot of relative distance between particles A and C and relative sizes of particles A and B in Fig. 8 vs the "relative tilt angle." For this plot, all distances and diameters were normalized to the AC distance found at +35° tilt, and the abscissa refers to the number of degrees of tilt relative to the upper limit of the tilt stage; i.e., a tilt angle of +35° is zero on the graph, while −35° is 70° on the graph. (+) Predicted distance based on cosine rule; (△) actual relative distance AC found; (○, ■) relative diameter of particles A and B, respectively, normalized to the diameters found at +35° tilt.

ing more rough and inhomogeneous than following the oxidation (Fig. 13). This can also be seen clearly in a side view of the re-reduced particle in Figs. 3 and 6, as shown in Fig. 14. Size comparisons between the oxidized and re-reduced particles did not shown any large changes in the diameter of the particles as a result of re-reduction.

DISCUSSION

The basic model of particle structure determined on the basis of the work done in this study is shown in Fig. 15. In brief, it is postulated that following reduction at 673 K in H_2 spherical particles which consist of an Fe core and a MnO outer layer form. During oxidation two major processes occur: Fe ions diffuse into the MnO structure, converting it into Fe_2MnO_4 or a mixed $Fe_{2-x}Mn_xO_4$ spinel, and also some Fe ions diffuse all the way through the MnO layer to the exterior of the particle where they are oxidized. This leads to the formation of an α-Fe_2O_3 outer layer on the particles, which spreads over the MnO surface. Diffusion of Fe ions from the particle center leaves a metastable void space. During re-reduction, the Fe and Mn again phase separate; however, the final morphology is different than that found following the first reduction. The void spaces in the particle centers remain largely intact during this re-reduction. The major aspects of the model are explained below on the basis of the present data, earlier studies on Fe–Mn systems, and the known mechanism of Fe oxidation.

Initial Reduction

On the basis of the results obtained in this study and previously published information, it is very reasonable to propose that

FIG. 10. Micrograph of Mn-only catalyst after oxidation at 523 K and air exposure at 300 K. Note that no void space formed in these particles. The particle sizes did not change as a result of the oxidation pretreatment.

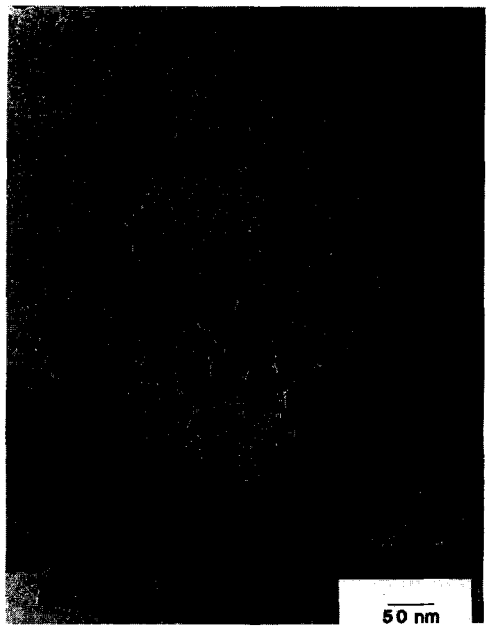

FIG. 11. Micrograph of Fe-only catalyst after oxidation at 523 K and air exposure at 300 K; same group of particles as in Fig. 4. Void spaces formed in all particles, and a quantitative summary of a tilt series is shown in Fig. 12.

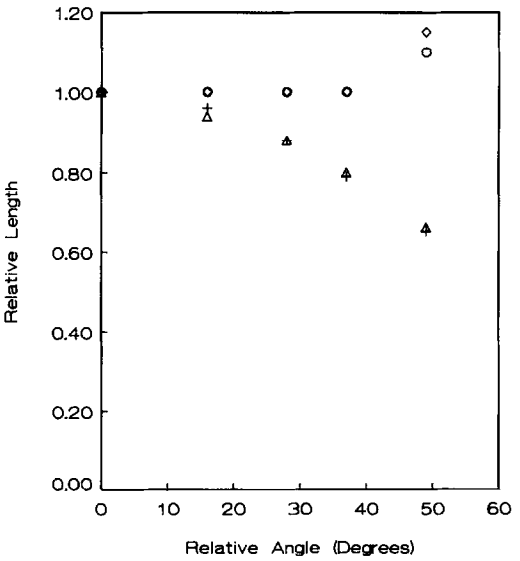

FIG. 12. Summary graph of tilting for the Fe-only sample after oxidation at 523 K. (+) Predicted normalized distance based on the cosine rule; (△) actual relative distance D1 found; (○) relative diameter of particle A; (◇) relative diameter of particle B.

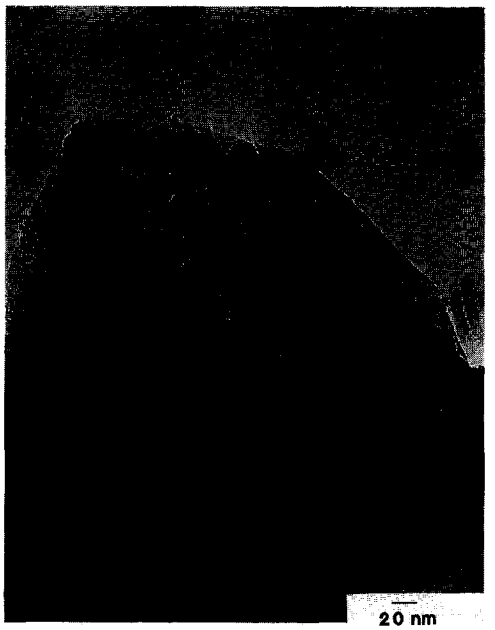

FIG. 13. Micrograph of catalyst after oxidation and re-reduction in H_2 at 673 K for 16 h. Note the irregular surface of the particle in the center of the picture.

following the initial reduction, the Fe–Mn particles are spherical with MnO outer shells and metallic Fe cores. Fe–Mn phase separation and surface MnO enrichment during the high-temperature reduction of Fe–Mn particles and films have been previously observed by several workers (*3, 10, 11, 14, 29*). In the present study the MES results confirm that phase separation occurs with these particles, and it is postulated that the surface is enriched in Mn oxide, presumably MnO, following the initial reduction. The TEM tilting experiments strongly support a spherical particle geometry, since no particle foreshortening was detected, and tilting had no effect on the apparent circular shape of the particles. It is reasonable to anticipate that the particles would be spherical on a graphitic support, as it has been repeatedly shown that metal–graphite interactions are extremely weak (*18, 24, 26*). Despite the fact that the Fe and Mn do not exist in a homogeneous phase,

FIG. 14. Micrograph of the same particle as that in Figs. 3 and 7 after oxidation and re-reduction at 673 K. This edge view was taken at a higher magnification than the micrographs in Figs. 3 and 7 to show the irregular structure of the surface. No noticeable change in the overall size of the particle was noted after re-reduction.

EDS results indicate that the Fe and Mn do not tend to form separate monometallic particles. Instead, both components are present in each particle, presumably in the form of Mn oxide covering an Fe core.

Oxidation

The proposition that the particles continue to be spherical following oxidation is again justified by the tilting experiments (see, for example, Figs. 7 and 8), by the fact that the particle appearance is independent of tilt angle, and by the side views of the particles (Fig. 7). The ring-like appearance is not an artifact due to diffraction. Previous investigations have shown that thickness fringes can appear on solid particles of spherical shape at certain tilt angles due to diffraction (*30*). In this study, however, the oxidized particles remained constant in their appearance at all tilt angles.

Instead, it is suggested that the ring-like appearance results from a *hollow core*. There is precedent for this suggestion. Recent work (*31*) with small silica-supported Rh particles showed that those particles, which are similar in appearance to the particles observed here, have a hollow center following reduction. Thus, there is precedent for the suggestion that particles which appear ring-like (or toroidal) in the TEM have a hollow center.

The suggestion that the particles have a hollow center is further supported by the measured increase in the particle diameter following oxidation. Consider the case where a metal particle exists as a sphere of metallic Fe surrounded by a uniform MnO shell, with an overall Fe/Mn ratio of 2/1. During oxidation, if the particle is converted to a solid sphere of Fe_2O_3 covered by a shell of Mn_2O_3, the predicted diameter expansion will be approximately 20%, on the basis of the known densities of the respective metals and oxides. Alternatively,

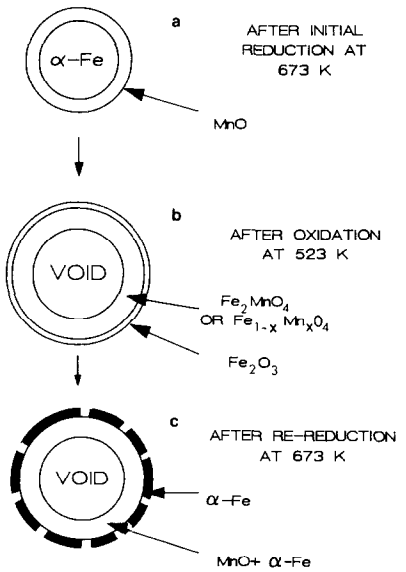

FIG. 15. Proposed geometry and phase structure of Fe–Mn particles as a result of reducing and oxidizing pretreatments. (a) Following reduction at 673 K. (b) After oxidation at 523 K. (c) After re-reduction at 673 K.

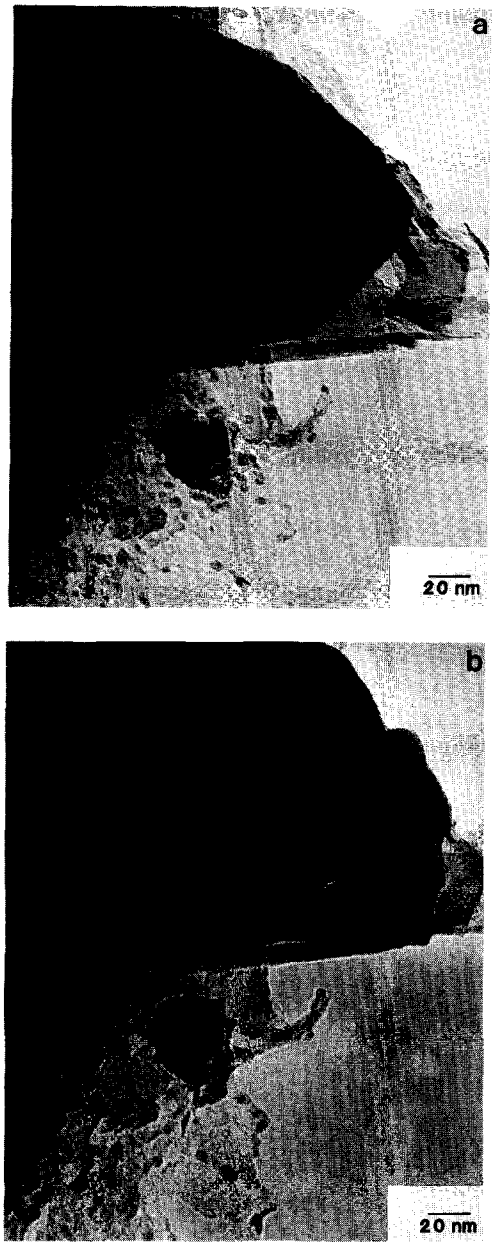

FIG. 16. Photomicrograph of a large Fe–Mn particle (a) after reduction at 673 K and air exposure at 300 K, (b) after oxidation at 523 K and air exposure at 300 K. Note that the particle interior in (b) has the shape of the exterior of the particle in (a) after reduction.

if the Fe–MnO particle is converted to a homogeneous sphere of Fe_2MnO_4, the expansion will be only about 17%. Clearly, these values are too low to explain the 39% increase observed in this study. From the standpoint of volume expansion, the differences are even more dramatic; oxidation to a solid sphere of oxide will be accompanied by a volume expansion of 73% whereas a volume expansion of approximately 268% was found for the particles in this study.

Pictures of the oxidation process for the large Fe–Mn particle in Fig. 16 support the premise that material from the interior of the particles diffuses out during oxidation. As seen in Fig. 16b, the original outline of the particle is retained, but it is surrounded by an irregularly shaped layer of material following oxidation. If oxidation had occurred uniformly throughout the particle, the particle would have expanded, but it would have retained the same exterior shape as the reduced particle.

In the model presented in this work, it is proposed that during oxidation Fe ions diffuse through the MnO layer to the surface where they react with oxygen. This is reasonable for Fe given the general understanding that in codiffusional processes the smaller species dominates which, considering the relative sizes of oxygen anions and Fe cations, is Fe in this case. Indeed, a recent investigation shows that Fe^{2+} cations are quite mobile through oxide layers at temperatures above 373 K (*32*). Also, there are several previous studies which show cavities forming during iron oxidation (*33–35*). For example, during the oxidation of highly curved surfaces such as Fe wires, previous investigations (*36, 37*) have shown that voids formed between the outer oxide layer and the metallic Fe core at temperatures below 1075 K. These studies further illustrate that the model proposed in the present work is not without precedent.

In order to explain the MES and XRD data obtained following oxidation, one may propose that the MnO layer is converted to a layer of Fe_2MnO_4 or possibly nonstoichiometric $Fe_{2-x}Mn_xO_4$. This seems reasonble given that Fe ions are thought to be diffusing through the (initially) MnO layer during the oxidation process.

The discussion concerning oxidation applies to the large particles which do not contain voids just after reduction. For small particles less than 10 nm in diameter, it is proposed that exposure to air at room temperature (during transfer to the TEM) leads to the formation of similar hollow structures by the same mechanism. Because of their small size, it is reasonable to assume that complete oxidation of these particles takes place in a very short time. The proposal that the small particles were oxidized following air exposure after the initial reduction, but just prior to examination in the TEM, is consistent with the observation that these small particles remain constant in size despite the subsequent high-temperature oxidation.

For the Fe-only catalyst, the morphology changes caused by oxidation were the same as those for the Fe–Mn catalyst, i.e., a large particle expansion and the formation of a void space in the particle interior. The model postulated for the Fe–Mn sample is still applicable to the Fe-only case, and, as mentioned earlier, experimental results have shown that voids form during the oxidation of Fe-only materials (*36, 37*).

The behavior of the Mn-only sample is not explainable by the same model as that for the Fe and Fe–Mn samples. The fact that the Mn particles do not change after the oxidation treatment implies that they were fully oxidized even after the initial reduction pretreatment. Previous results have indicated that the reduction of Mn oxide to zero-valent Mn is very unlikely under the conditions used here (*4*). Thus there would have been no driving force for the diffusion of Mn cations during oxidation, as all of the Mn is already oxidized. The proposal that the Mn stays oxidized is completely consistent with the lack of particle growth and the absence of voids in the Mn-only sample after oxidation.

There have been numerous reports of "pitted" or "toroidal" particles forming during the reduction and oxidation of metal particles (*31, 38–47*). In several previous studies, supported metal particles which appeared to be ring-like in the TEM were assumed to be toroidal in structure (*38–43*). That is, it was assumed that they consisted of a thin layer of metal in the center and a thick ring of metal on the outside. Possibly, the "toroidal" particles seen in these studies were actually hollow spheres. Indeed, tilting experiments were not performed in any of those studies. Furthermore, in virtually all cases workers suggested that the toroidal shapes were a consequence of a strong interaction between the metal particle and the support, although the details of the models differed (*39, 40, 42*). No model which requires a strong metal–support interaction can reasonably apply in the present case as all the evidence in both this study (e.g., large particles) and previous studies (*26*) suggests that metal–graphite interactions are weak.

Re-reduction

Upon re-reduction at 673 K, there is no change in particle size and the particles still appear hollow, but the particle surface appears to be very inhomogeneous (Figs. 13, 14). The exact cause for this is unknown; however, one possible explanation is that a fracturing of the surface could have occurred as a result of the reduction of Fe_2O_3 to Fe while it is in contact with Mn oxide. This explanation assumes that a thin layer of Fe_2O_3 exists on the particle exterior following the oxidation process. In CO hydrogenation results reported elsewhere (*48*), the re-reduced surface does give selectivities and activities most characteristic of unpromoted Fe, which supports the idea of an Fe_2O_3 overlayer just prior to the re-reduction. If this is so, the oxide layer may have spread over the Fe–Mn mixed oxide layer; this spreading would be analogous to the cases where metal oxides spread over oxidic supports (*39, 40, 46*), with the Fe–Mn oxide acting as the "support." During re-reduction, the elimination of O from Fe_2O_3 would contract the outer Fe layer to a larger extent than the underlying oxide

layer, which would presumably exist as MnO after reduction. The resulting shrinkage of the Fe_2O_3 shell would lead to the fracturing observed. Further studies are needed to confirm this last hypothesis.

SUMMARY

Reduction and oxidation pretreatments can greatly influence the structure of Grafoil-supported Fe–Mn particles. Following an initial reduction, MES results, TEM tilting experiments, and previous results from the literature suggest that the particles exist as a sphere of Fe covered with a layer of MnO. Subsequent high-temperature oxidation of the particles causes them to assume a hollow spherical geometry, and both Fe and Fe–Mn oxides were detected. The formation of the mixed oxide is postulated to take place as a result of the outward diffusion of Fe cations, a mechanism of oxidation which is well known and also accounts for the formation of a void in the center of the metal particles. Re-reduction of the oxidized particles causes a breakup of the particle surface, and a large portion of the Fe in the mixed oxide phase separates to form α-Fe.

The simplicity of this model suggests that it may be applicable to systems other than Fe and Fe–Mn including systems in which particles were previously reported to be toroidal. In fact, it should be valid in any system where metal oxidation occurs via the diffusion of metal ions through an oxide layer. As demonstrated, TEM tilting experiments provide a straightforward means of determining whether the particles are spherical in shape or actually toroids.

ACKNOWLEDGMENTS

This study was supported by the NSF Kinetics and Catalysis Program via Grant CBT-8619619. Partial support of A. A. Chen by a Texaco Philanthropic Foundation Fellowship is gratefully acknowledged. The authors thank Dr. George Wagner for synthesizing the carbonyl cluster precursor used in this study.

REFERENCES

1. Koelbel, H., and Tillmetz, K. D., U.S. Patent 4,177,203 (1979).
2. Bussmeier, B., Frohning, C. D., and Cornils, B., *Hydrocarbon Process.* **11,** 105 (1976).
3. Kreitman, K., Baerns, M., and Butt, J. B., *J. Catal.* **105,** 319 (1987).
4. Venter, J., Kaminsky, M., Geoffroy, G. L., and Vannice, M. A., *J. Catal.* **103,** 450 (1987).
5. Jaggi, N. K., Schwartz, L. H., Butt, J. B., Papp, H., and Baerns, M., *Appl. Catal.* **13,** 347 (1985).
6. Maiti, G. C., Malessa, R., and Baerns, M., *Appl. Catal.* **5,** 151 (1983).
7. Maiti, G. C., Malessa, R., Lochner, U., Papp, H., and Baerns, M., *Appl. Catal.* **16,** 215 (1985).
8. Kolk, B., Albers, A., Leith, I. R., and Howden, M. G., *Appl. Catal.* **37,** 57 (1988).
9. Leith, I. R., and Howden, M. G., *Appl. Catal.* **37,** 75 (1988).
10. Benecke, W., Schulz, R., Feller, H. G., and Ralek, M., "Proceedings, 8th International Congress on Catalysis, Berlin, 1984," Vol. 2, p. 219. Dechema, Frankfurt-am-Main, 1984.
11. Grzybek, T., Papp, H., and Baerns, M., *Appl. Catal.* **29,** 351 (1987).
12. Deppe, P., Papp, H., and Rosenberg, M., *Hyperfine Interact.* **28,** 903 (1986).
13. Lochner, U., Papp, H., and Baerns, M., *Appl. Catal.* **23,** 339 (1986).
14. Jensen, K. B., and Massoth, F. E., *J. Catal.* **92,** 98 (1985).
15. Van Dijk, W. L., Niemantsverdriet, J. W., Van Der Kraan, A. M., and Van Der Baan, H. S., *Appl. Catal.* **2,** 273 (1982).
16. Gatte, R. R., and Phillips, J., *J. Phys. Chem.* **91,** 5961 (1987).
17. Morup, S., Dumesic, J. A., and Topsøe, H., *in* "Applications of Mössbauer Spectroscopy" (R. L. Cohen, Ed.), Vol. 2, p. 1. Academic Press, New York, 1980.
18. Phillips, J., Clausen, B., and Dumesic, J. A., *J. Phys. Chem.* **84,** 1814 (1980).
19. Bretz, M., Dash, J. G., Hickernell, D. C., McLean, E. O., and Vilches, O. E., *Phys. Rev. A* **8,** 1589 (1973).
20. Bukshpan, S., Sonnino, T., and Dash, J. G., *Surf. Sci.* **52,** 460 (1975).
21. Kjems, J. K., Passell, L., Taub, H., Dash, J. G., and Novao, A. D., *Phys. Rev. B* **13,** 1446 (1976).
22. Ruff, J. K., *Inorg. Chem.* **7,** 1818 (1968).
23. Shriver, D. F., and Drezdon, M. A., "The Manipulation of Air-Sensitive Compounds," 2nd ed. Wiley, New York, 1986.
24. Lin, S.-C., and Phillips, J., *J. Appl. Phys.* **58,** 1943 (1985).
25. Sorenson, K., Internal Report No. 1, Laboratory of Applied Physics, Technical University of Denmark, Lyngby, Denmark, 1972.
26. Wu, N. L., and Phillips, J., *Surf. Sci.* **184,** 463 (1987).
27. Baker, R. T. K., France, J. A., Rouse, L., and Waite, R. J., *J. Catal.* **41,** 22 (1976).

28. Gatte, R. R., and Phillips, J., *J. Catal.* **104,** 365 (1987).
29. Benecke, W., Feller, H. G., and Ralke, M., *Z. Metal.* **75,** 625 (1974).
30. Treacy, M. M., and Howie, A., *J. Catal.* **63,** 265 (1980).
31. Chakraborti, S., Dayte, A. K., and Long, N. J., *J. Catal.* **108,** 444 (1987).
32. Langell, M., and Somorjai, G. A., *J. Vac. Sci. Technol.* **21,** 858 (1982).
33. Kubaschewski, O., and Hopkins, B. E., "Oxidation of Metals and Alloys," 2nd ed., pp. 95–108. Butterworths, London 1967.
34. Wagner, C., *in* "Atom Movements," p. 153. American Society for Metals, Cleveland, 1951.
35. Brophy, J. H., Rose, R. M., and Wulff, J., "The Structure and Properties of Materials," Vol. 2, pp. 148–151. Wiley, New York, 1964.
36. Engell, H., and Wever, F., *Acta. Metall.* **5,** 695 (1957).
37. Dunnington, B. W., Beck, F. H., and Fontana, M. G., *Corrosion* **8,** 2 (1952).
38. Nakayama, T., Arai, M., and Nishiyama, Y., *J. Catal.* **87,** 108 (1984).
39. Derouane, E. G., Chludzinski, J. J., and Baker, R. T. K., *J. Catal.* **85,** 187 (1984).
40. Nakayama, T., Arai, M., and Nishiyama, Y., *J. Catal.* **79,** 497 (1983).
41. Ruckenstein, E. E., and Chen, J. J., *J. Colloid Interface Sci.* **86,** 1 (1982).
42. Tatarchuk, B. J., Chludzinski, J. J., Sherwood, R. D., Dumesic, J. A., and Baker, R. T. K., *J. Catal.* **70,** 433 (1981).
43. Sushumna, I., and Ruckenstein, E., *J. Catal.* **90,** 241 (1984).
44. Wang, T., and Schmidt, L. D., *J. Catal.* **70,** 187 (1981).
45. Chen, J. J., and Ruckenstein, E., *J. Catal.* **69,** 257 (1981).
46. Chen, J. J., and Ruckenstein, E., *J. Phys. Chem.* **85,** 1606 (1981).
47. Arai, M., Nakayama, T., and Nishiyama, Y., *J. Catal.* **111,** 440 (1988).
48. Chen, A. A., Ph.D. thesis, The Pennsylvania State University, 1988.
49. Weiser, E., Meisel, W., and Kleinstuck, K., *Phys. Status Solidi* **16,** 127 (1966).
50. Tanaka, M., Mizoguchi, T., and Aiyama, Y., *J. Phys. Soc. Japan* **18,** 1091 (1963).
51. Bunget, I., *Phys. Status Solidi* **28,** K39 (1968).
52. Bauminger, R., Cohen, S. G., Marinov, A., Ofer, S., and Segal, E., *Phys. Rev.* **122,** 1447 (1961).
53. Armstrong, R. J., Morrish, A. H., and Sawatzky, G. A., *Phys. Lett.* **23,** 7 (1966).
54. Kelly, W. H., Folen, V. J., Hass, M., Schreiner, W. N., and Beard, G. B., *Phys. Rev.* **124,** 80 (1961).
55. Van der Woude, F., *Phys. Status Solidi* **17,** 417 (1966).